PHYSICAL REVIEW E **105**, 064408 (2022)

Effect of vibrational modes on electron transfer directionality: Photosynthetic reaction centers

Michal Pudlák,[1,*] Richard Pinčák,[1,†] and Erik Bartoš[2,‡]
[1]Institute of Experimental Physics, Slovak Academy of Sciences, Watsonova 47, 043 53 Košice, Slovak Republic
[2]Institute of Physics, Slovak Academy of Sciences, Dúbravská Cesta 9, 845 11 Bratislava, Slovak Republic

(Received 8 March 2022; accepted 25 May 2022; published 10 June 2022)

It is shown in the example of the photosynthetic reaction centers (RCs) that the electron transfer can be directed by vibrational modes into the needed site where it is localized. In the case of the RC, it is the low vibrational mode that produces such an effect. We find that the electron transfer unidirectionality in the photosynthetic reaction center can be determined by the asymmetry in the reorganization energy of the vibrational modes at high temperatures. We also numerically solve generalized master equations for various vibration relaxation times. The results are compared with the solution of master equations. It is shown that for small relaxation times, the non-Markovian electron transfer kinetics gives similar results as the Markovian approximation, but the results are significantly different for the long vibration relaxation times.

DOI: 10.1103/PhysRevE.105.064408

I. INTRODUCTION

Light-induced charge transfer from the photoexcited donor to the acceptor is a fundamental step that has to be understood in detail to generate solar cells of high efficiency. Although there are structural and functional differences, the laws that govern quantum solar energy conversion into chemical energy in biological systems, either into electricity in semiconductor solar cells, share many similarities [1,2]. In these systems, the conversion processes proceed from the creation of electron-hole pairs (excitons) by a photon of light, followed by charge separation to produce the required high-energy product. The methods and technologies for the efficient conversion of sunlight into electricity are the key challenges in current energy research [3]. The charge transfer is mediated by many degrees of freedom, and some of them are only partially controlled. The lack of control is summarized as disorder or noise inflicted on the transport process of interest [4]. Quantum dissipation plays an important role in understanding quantum dynamics processes. The interaction between a quantum system and the environment causes the loss of the energy and coherence of the quantum system. The essential task is to describe the system of interest in the proper way, where all necessary conditions are taken into account. The approach, where the master equations to second order, which can be generalized to the higher order of the perturbation theory, and not limited to the harmonic bath assumption, is presented in Refs. [5,6].

The main goal of the present paper is to evaluate the effect of the vibration modes on electron transfer (ET) directionality and charge separation. We assume that the incoming energy excites an electron out of a low-energy state, across the energy gap, into a high-energy excited state. Subsequently begins the electron transfer reaction where the electron-vibration coupling plays an important rational role. The dynamics of an open quantum system is expected to deviate from the Markovian approximation. The standard approach to the dynamics of an open system uses the Nakajima-Zwanzig projection operator technique. It was shown that a real system possesses memory [7,8]. In dependence on the memory character, the dynamics of the quantum system are coherent, incoherent, or some kind of mixed regime between the previous mention dynamics. The terminal examples are (i) the constant memory functions, which means the infinite memory, and so we get the coherent motion, and (ii) the memory function has a delta function character and so zero memory; the system dynamics is incoherent. The actual systems can operate between these two regimes.

In this paper, the role of electron-vibration interaction on the electron transfer directionality is investigated. We also study the non-Markovian dynamics of the system and compare the results with the results obtained in the Markovian approximation.

II. GENERALIZED MASTER EQUATION FOR CHARGE TRANSFER PROCESSES

Formally, an exact generalized master equation (GME) which describes the electron transfer processes in systems with dissipation can be constructed utilizing the projection operator techniques. Specifically, let us consider a system in which an electron has N accessible sites embedded in a medium. Such a system is described by the Hamiltonian

$$H = H_0 + V, \tag{1}$$

where $H_0 = \sum_{n=1}^{N} |n\rangle[\varepsilon_n - i\Gamma_n + H_n^v]\langle n|$. Here, $|n\rangle$ is the electron state with energy ε_n. The parameter $\hbar/2\Gamma_n$ characterizes the electron lifetime at site $|n\rangle$. It may originate, for example, from a recombination process. These parameters

---

[*] pudlak@saske.sk

[†] pincak@saske.sk

[‡] erik.bartos@savba.sk

also describe the interaction of the system of interest with another part of the whole system from which the backward electron transfer is not possible in real time. The term H_n^v describes a medium consisting of harmonic oscillators:

$$H_n^v = \sum_a \left\{ \frac{p_\alpha^2}{2m_\alpha} + \frac{1}{2} m_\alpha \omega_\alpha^2 (q_\alpha - d_{n\alpha})^2 \right\}. \tag{2}$$

Here, $d_{n\alpha}$ is the equilibrium configuration of the α th oscillator, which depends on the electronic state $|n\rangle$. The interaction $V = \sum_{n,m=1}^N V_{nm} |n\rangle\langle m| (n \neq m)$ couples different sites of the electron localization.

The GME formulation of an electron (an exciton) interacting with vibrational modes (phonons) starts from the Liouville equation for a density operator $\rho(t)$:

$$i \frac{\partial}{\partial t} \rho(t) = \frac{1}{\hbar} [H\rho(t) - \rho(t) H^+] \equiv L\rho(t). \tag{3}$$

The projector operator confines the full information about the system into the relevant one. Our prime interest is the information about the electron localization and the irrelevant information is a particular vibrational state excited in the system. In virtue of this technique [7,8], one obtains

$$\begin{aligned} \frac{\partial}{\partial t} D\rho(t) &= -iDLD\rho(t) - \int_0^t DL \exp[-i(1-D)L\tau] \\ &\quad \times (1-D)LD\rho(t-\tau) d\tau \\ &\quad - iDL \exp[-i(1-D)Lt](1-D)\rho(0) \end{aligned} \tag{4}$$

for the relevant part $D\rho(t)$ of the total density $\rho(t)$. Here $D = D^2$ is an arbitrary linear projection operator which can be used in the form [9]

$$DA = \sum_n \mathrm{Tr}(\ |n\rangle\langle n|\ A\ ) \rho_n |n\rangle\langle n|. \tag{5}$$

The total trace $\mathrm{Tr} = \mathrm{Tr}_e \mathrm{Tr}_Q$ is a product of traces of the electronic (Tr_e) and the vibrational (Tr_Q) subsystems; $\rho_n = \exp(-\beta H_n^v)/\mathrm{Tr}_Q[\exp(-\beta H_n^v)]$ is a density operator for a vibrational subsystem, when an electron is localized at a site $|n\rangle$ ($\beta = 1/k_B T$). We assume that the initial term $(1-D)\rho(0) = 0$. It means that the electron and phonon subsystems are initially in equilibrium. Substituting Eq. (5) in Eq. (4), one obtains the GME

$$\begin{aligned} \partial_t P_n(t) = -\frac{2\Gamma_n}{\hbar} P_n(t) - \sum_{m(\neq n)} \int_0^t [&\mathrm{Re} W_{nm}(t-\tau) P_n(\tau) \\ &- \mathrm{Re} W_{mn}(t-\tau) P_m(\tau)] d\tau \end{aligned} \tag{6}$$

for site-occupation probabilities:

$$P_n(t) = Tr(\ |n\rangle\langle n|\ \rho(t)\ ) = \rho_{nn}(t). \tag{7}$$

The first term in the r.h.s. of Eq. (6) is associated with the probability for an electron to escape from the system via an additional channel. The memory function $W_{mn}(t)$ can be expressed in the form

$$\begin{aligned} W_{mn}(t) &= 2\frac{|V_{mn}|^2}{\hbar^2} \exp\left(-\frac{\Gamma_m + \Gamma_n}{\hbar} t\right) \\ &\quad \times \exp\left(i\frac{\varepsilon_{mn}}{\hbar} t\right) \exp\left(\sum_\alpha -\frac{E_{mn}^\alpha}{\hbar\omega_\alpha} \mathcal{N}_\alpha(t)\right). \end{aligned} \tag{8}$$

Here

$$\varepsilon_{mn} = \varepsilon_m - \varepsilon_n \tag{9}$$

and

$$E_{mn}^\alpha = \tfrac{1}{2} m_\alpha \omega_\alpha^2 (d_{m\alpha} - d_{n\alpha})^2 \tag{10}$$

is the reorganization energy of the α th vibrational mode, when an electron moves from state $|m\rangle$ to state $|n\rangle$,

$$\mathcal{N}_\alpha(t) = (2\bar{n}_\alpha + 1)(1 - \cos\omega_\alpha t) + i \sin\omega_\alpha t \tag{11}$$

and $\bar{n}_\alpha = [\exp(\hbar\omega_\alpha/k_B T) - 1]^{-1}$ is a thermal population of the α th vibrational mode.

III. THE ELECTRON TRANSFER DIRECTIONALITY

We start with the examination of the electron transfer within a three-site model. We assume similarly to the photosynthetic reaction centers (RCs) that after photon absorption at site 1 the electron transfer may occur either through site 2 or site 3. We assume that there are two nonzero coupling terms V_{12} and V_{13} and a forbidden direct electron transfer between molecules 2 and 3 ($V_{23} = 0$). We describe the electron transport in three-site systems by the following kinetic model:

$$\begin{aligned} \partial_t P_1(t) &= -\frac{2\Gamma_1}{\hbar} P_1(t) - \sum_{j=2,3} \int_0^t [\mathrm{Re} W_{1j}(t-\tau)] P_1(\tau) d\tau \\ &\quad + \sum_{j=2,3} \int_0^t [\mathrm{Re} W_{j1}(t-\tau)] P_j(\tau) d\tau, \end{aligned} \tag{12}$$

$$\begin{aligned} \partial_t P_2(t) &= -\frac{2\Gamma_2}{\hbar} P_2(t) - \int_0^t [\mathrm{Re} W_{21}(t-\tau)] P_2(\tau) d\tau \\ &\quad + \int_0^t [\mathrm{Re} W_{12}(t-\tau)] P_1(\tau) d\tau, \end{aligned} \tag{13}$$

$$\begin{aligned} \partial_t P_3(t) &= -\frac{2\Gamma_3}{\hbar} P_3(t) - \int_0^t [\mathrm{Re} W_{31}(t-\tau)] P_3(\tau) d\tau \\ &\quad + \int_0^t [\mathrm{Re} W_{13}(t-\tau)] P_1(\tau) d\tau. \end{aligned} \tag{14}$$

Now we compute the quantum yields of the electronic escape via the molecules $3(\Phi_3)$ and $2(\Phi_2)$ and the quantum yields Φ_G of the direct ground-state recombination. These quantities can be characterized by the expressions

$$\Phi_G = \frac{2\Gamma_1}{\hbar} \int_0^\infty P_1(t) dt = \frac{2\Gamma_1}{\hbar} \bar{P}_1(s \mapsto 0^+), \tag{15}$$

$$\Phi_2 = \frac{2\Gamma_2}{\hbar} \int_0^\infty P_2(t) dt = \frac{2\Gamma_2}{\hbar} \bar{P}_2(s \mapsto 0^+), \tag{16}$$

$$\Phi_3 = \frac{2\Gamma_3}{\hbar} \int_0^\infty P_3(t) dt = \frac{2\Gamma_3}{\hbar} \bar{P}_3(s \mapsto 0^+), \tag{17}$$

where $\bar{P}_i(s)$ is the Laplace transformation of $P_i(t)$:

$$\bar{P}_i(s) = \int_0^\infty e^{-st} P_i(t) dt. \tag{18}$$

The Laplace transform to Eqs. (12)–(14), with the initial conditions $P_1(0) = 1$, $P_2(0) = 0$, $P_3(0) = 0$, reads

$$s\bar{P}_1(s) - 1 = -\left(\frac{2\Gamma_1}{\hbar} + \bar{W}_{12}(s) + \bar{W}_{13}(s)\right)\bar{P}_1(s) + \bar{W}_{21}(s)\bar{P}_2(s) + \bar{W}_{31}(s)\bar{P}_3(s), \tag{19}$$

$$s\bar{P}_2(s) = -\left(\frac{2\Gamma_2}{\hbar} + \bar{W}_{21}(s)\right)\bar{P}_2(s) + \bar{W}_{12}(s)\bar{P}_1(s), \tag{20}$$

$$s\bar{P}_3(s) = -\left(\frac{2\Gamma_3}{\hbar} + \bar{W}_{31}(s)\right)\bar{P}_3(s) + \bar{W}_{13}(s)\bar{P}_1(s), \tag{21}$$

where

$$\bar{W}_{mn}(s) = 2\frac{|V_{mn}|^2}{\hbar^2}\mathrm{Re}\int_0^\infty \exp\left(-\frac{\Gamma_m + \Gamma_n + \hbar s}{\hbar}t\right) \times \exp\left(i\frac{\varepsilon_{mn}}{\hbar}t\right)\exp\left(\sum_\alpha -\frac{E^\alpha_{mn}}{\hbar\omega_\alpha}\mathcal{N}_\alpha(t)\right)dt. \tag{22}$$

Using the solutions of Eqs. (19)–(21), we get

$$\Phi_G = \frac{2\Gamma_1}{\hbar}\frac{1}{\mathcal{P}}, \tag{23}$$

$$\Phi_2 = \frac{1}{\mathcal{P}}\frac{k_{12}}{1 + k_{21}\frac{\hbar}{2\Gamma_2}}, \tag{24}$$

$$\Phi_3 = \frac{1}{\mathcal{P}}\frac{k_{13}}{1 + k_{31}\frac{\hbar}{2\Gamma_3}}, \tag{25}$$

where

$$\mathcal{P} = \frac{2\Gamma_1}{\hbar} + \frac{k_{12}}{1 + k_{21}\frac{\hbar}{2\Gamma_2}} + \frac{k_{13}}{1 + k_{31}\frac{\hbar}{2\Gamma_3}}. \tag{26}$$

Here we denote $\bar{W}_{ij}(s \to 0^+)$ as k_{ij}. The constant k_{ij} can be computed now. We use the two-phonon mode approximation that previously characterized the electron transfer reactions in the biological systems:

$$k_{ij} = 2\mathrm{Re}\frac{|V_{ij}|^2}{\hbar^2}\int_0^\infty \exp\left(-\frac{\Gamma_i + \Gamma_j}{\hbar}t\right) \times \exp\left(i\frac{\varepsilon_{ij}}{\hbar}t\right)\exp\left(\sum_{\alpha=h,v} -\frac{E^\alpha_{ij}}{\hbar\omega_\alpha}\mathcal{N}_\alpha(t)\right)dt. \tag{27}$$

After integration, we get

$$k_{ij} = \frac{|V_{ij}|^2}{\hbar^2\omega_h}\exp\left(-S^h_{ij}(2\bar{n}_h + 1)\right)\exp\left(-S^v_{ij}(2\bar{n}_v + 1)\right) \times \sum_{q=-\infty}^{\infty}\sum_{p=-\infty}^{\infty}\left(\frac{\bar{n}_h + 1}{\bar{n}_h}\right)^{q/2} I_{|q|}\left[2S^h_{ij}\sqrt{\bar{n}_h(\bar{n}_h + 1)}\right] \times \left(\frac{\bar{n}_v + 1}{\bar{n}_v}\right)^{p/2} I_{|p|}\left[2S^v_{ij}\sqrt{\bar{n}_v(\bar{n}_v + 1)}\right] \times \frac{2(\Gamma_i + \Gamma_j)/\hbar\omega_h}{\left(\frac{\Gamma_i+\Gamma_j}{\hbar\omega_h}\right)^2 + \left(\frac{\varepsilon_{ij}}{\hbar\omega_h} - q\frac{\omega_v}{\omega_h} - p\right)^2}. \tag{28}$$

Here I_q are modified Bessel functions.

IV. PHOTOSYNTHETIC REACTION CENTER

The photosynthetic RC of bacteria provides an interesting and important system for studying a high-efficiency electron transfer in an organized molecular complex. The RC is a special pigment-protein complex that functions as a photochemical trap, which in such systems, after excitation, follows the fast electron transfer. All molecules (cofactors) involved in the ET are noncovalently bound to subunits L and M in two chains [10]. Both chains of cofactors start at the bacteriochlorophyll dimer (P) that interacts with both subunits L and M. The dimer plays the role of the donor of an electron (a weakly bound exciton) after the photon absorption. Cofactors in the subunit L are accessory bacteriochlorophyll ($\mathrm{BChl_L}$), bacteriopheophytin ($\mathrm{BPh_L}$) and quinone (Q_L). Identically, in the M subunit, there are the accessory bacteriochlorophyll ($\mathrm{BChl_M}$), bacteriopheophytin ($\mathrm{BPh_M}$) and quinone (Q_M). The cofactors serve as donor-acceptor pairs in the ET. The arrangement of cofactors shows the local twofold symmetry which is almost perfect with the respect to the dimer. The part of the L subunit involved in the ET can be superimposed onto the corresponding part of the M subunit by a rotation of almost exactly 180° (for more details on structural arrangement, see Ref. [10]). In the primary charge transfer, an electron is transferred from the photoexcited dimer P, the starting point for a series of electron transfer reactions across the membrane, to the cofactors on subunit L, to $\mathrm{BChl_L}$, $\mathrm{BPh_L}$, Q_La, and Q_M. On the other hand, the chain located on subunit M is inactive in the ET. The highly asymmetric functionality, however, can be decreased by amino acid mutations or cofactor modification [11]. Generally, it is believed that the different types of RCs have a similar structure, where the high efficiency of solar energy conversion to the chemical is based on the common electronic properties [12]. However, there is one peculiarity in the electron transfer in the RC of *C. aurantiacus*. This RC contain Bacteriopheophytin (BPh) in the M branch, where Bacteriochlorophyll (BChl) molecule is placed in the *Rb. sphaeroides* RC [13]. The M branch is active in the RCs with cofactor modification where the BChl molecule is replaced by the BPh molecule. It is thought that this replacement lowers the energy of the accessory molecule that causes branch M to be active. This is not the case with *C. aurantiacus* RC where branch M is inactive. In Ref. [14], the incoherent model was used to describe the kinetics for the RC of *C.aurantiacus*. It was shown that the asymmetry in the hopping terms ought to be used to describe the experimental data. On the other hand, the results of Ref. [15] reinforce the view that the native configuration of RC promote ET to the L branch primarily by balancing the free energy of the charge-separated states. So the question is whether the asymmetry in hopping terms is the only possibility to explain the electron transfer kinetics in the *C. aurantiacus* RC. To investigate the electron transfer in RC of *C.aurantiacus*, the theory presented in the previous sections will be used. We would like to elucidate the quantum yields observed in this RC. The quantum yields are more sensitive to the first step of electron transfer [9]. So the three-site model is employed to explain the observed quantum yields in *C. aurantiacus* RC. It is assumed that the free energy of the $P^+\mathrm{BChl}^-_\mathrm{M}$ state in *Rb. sphaeroides* RCs is about 1000 cm^{-1} higher then the $P^+\mathrm{BPh}^-_\mathrm{M}$ state of *C. aurantiacus* RCs. In our abbreviation, site 2 is the

TABLE I. Computed quantum yields and $\tau_{ij} = 1/k_{ij}$ for *C. aurantiacus* RCs.

T	τ_{12}	τ_{21}	τ_{13}	τ_{31}	$\hbar/2\Gamma_{2,3}$	S^v_{12}	S^v_{13}	Φ_G	Φ_2	Φ_3
K	ps	ps	ps	ps	ps					
300	69	82	6.7	59	2.6	12	4	0.03	0.09	0.88
80	332	537	5.8	822	2.6	12	4	0.03	0.02	0.95
10	1024	1230	5.8	963	2.6	12	4	0.03	0.01	0.96
300	69	82	6.7	60	2.6	12	12	0.04	0.08	0.88
80	332	537	17	2632	2.6	12	12	0.09	0.04	0.87
10	1024	1230	24	3028	2.6	12	12	0.02	0.12	0.86
300	19	27	6.7	59	2.6	4	4	0.03	0.24	0.73
80	19	34	5.8	822	2.6	4	4	0.03	0.21	0.76
10	24	73	5.8	963	2.6	4	4	0.03	0.18	0.79

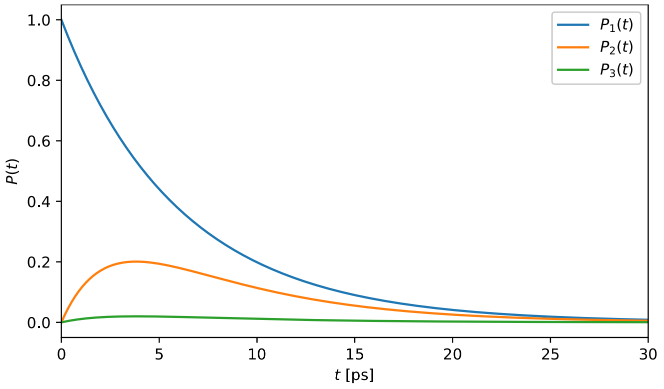

FIG. 1. The occupation probabilities $P_i(t)$ as a function of time t.

BPh$_M$ molecule, site 3 is the BChl$_\mathrm{L}$ molecule and site 1 is the bacteriochlorophyll dimer. So the free energy of site 2 cannot be high above the free energy of site 3 in *C. aurantiacus* RCs. The values $\varepsilon_{12} = 40$ cm^{-1} and $\varepsilon_{13} = 460$ cm^{-1} were used in these computations. The phonon bath is described by two vibrational modes, high-frequency mode ω_h, and low frequency ω_v. The low-frequency mode characterizes the exterior medium phonon mode and the high-frequency mode describes the molecular vibrational modes of the donor and the acceptor centers [16]. To explain the observed quantum yields in RCs of *C. aurantiacus*, we have to impose asymmetry in the reorganization energy of low-energy vibrational modes. We assume that reorganization energy $S^v_{12}\hbar\omega^v$ of the low-frequency mode related to electron transfer from site 1 to site 2 is bigger than the reorganization energy $S^v_{13}\hbar\omega^v$ related to electron transfer from site 1 to site 3. This assumption together with asymmetry in the free energy of sites 2 and 3 can elucidate the unidirectionality of the electron transfer in the *C. aurantiacus*. To demonstrate this, the following values of input parameters were used: the values of the scaled reorganization constants S^v_{12}, S^v_{13} using the computations defined in Table I, $S^h_{12} = S^h_{13} = 0.5$, high-frequency modes $\hbar\omega_h = 1500$ cm^{-1}, low-frequency mode $\hbar\omega_v = 80$cm^{-1}. The values for electronic coupling parameters $V_{12} = V_{13} = 48$ cm^{-1}. The P^* internal conversion rate is $2\Gamma_1/\hbar = (170\text{ ps})^{-1}$. In the numerical computations, the sink parameters $2\Gamma_2/\hbar = 2\Gamma_3/\hbar$. The calculated time $\tau_{ij} = 1/k_{ij}$ and quantum yields are collected in Table I. The observed kinetics and the quantum yields of the *C. aurantiacus* RCs can be elucidated using the asymmetry in the following two parameters: (i) free energies of sites 2 and 3 and (ii) reorganization energies of the low-frequency modes of the L andM protein subunits. This proposition is supported by the fact that there are differences in amino acid residues in the L and M protein subunits of *C. aurantiacus* RCs which differ from that in *Rb. sphaeroides* RCs [17]. Without the asymmetry in reorganization energies of low-frequency modes, both chains would be active. The computed constant τ_{13} that characterizes the electron transfer from bacteriochlorophyll dimer P to BChl$_\mathrm{L}$ the molecule in an open system is 6.7 ps at $T = 300$ K and 5.8 ps at $T = 80$ K. This is in accordance with experimental data presented in Ref. [18], where the temperature dependence of the initial electron-transfer kinetics in the RC of *C.aurantiacus* has been investigated. Now, assuming that the Markovian approximation can be done, we are solving the system of Eqs. (19)–(21), where instead of $W_{ij}(s)$ is k_{ij}. We get

$$\bar{P}_1(s) = \frac{\left(s + \frac{2\Gamma_3}{\hbar} + k_{13}\right)\left(s + \frac{2\Gamma_2}{\hbar} + k_{12}\right)}{(s - s_1)(s - s_2)(s - s_3)}, \tag{29}$$

$$\bar{P}_2(s) = \frac{k_{12}\left(s + \frac{2\Gamma_3}{\hbar} + k_{31}\right)}{(s - s_1)(s - s_2)(s - s_3)}, \tag{30}$$

$$\bar{P}_3(s) = \frac{k_{13}\left(s + \frac{2\Gamma_2}{\hbar} + k_{21}\right)}{(s - s_1)(s - s_2)(s - s_3)}. \tag{31}$$

where s_i, $i = 1, 2, 3$ are the solutions of the equation

$$s^3 + X_1 s^2 + X_2 s + X_3 = 0, \tag{32}$$

where

$$X_1 = \frac{2\Gamma_1}{\hbar} + \frac{2\Gamma_2}{\hbar} + \frac{2\Gamma_3}{\hbar} + k_{12} + k_{21} + k_{13} + k_{31} \tag{33}$$

$$\begin{aligned} X_2 &= \left(\frac{2\Gamma_2}{\hbar} + \frac{2\Gamma_3}{\hbar}\right)\left(\frac{2\Gamma_1}{\hbar} + k_{12} + k_{13}\right) \\ &\quad + \frac{2\Gamma_1}{\hbar}(k_{21} + k_{31}) + k_{31}k_{12} + k_{21}k_{13} \\ &\quad + \left(\frac{2\Gamma_2}{\hbar} + k_{21}\right)\left(\frac{2\Gamma_3}{\hbar} + k_{31}\right), \end{aligned} \tag{34}$$

$$\begin{aligned} X_3 = {}& \frac{2\Gamma_1}{\hbar}\left(\frac{2\Gamma_2}{\hbar} + k_{21}\right)\left(\frac{2\Gamma_3}{\hbar} + k_{31}\right) + \frac{2\Gamma_3}{\hbar}\left(\frac{2\Gamma_2}{\hbar} + k_{21}\right)k_{13} \\ & + \frac{2\Gamma_2}{\hbar}\left(\frac{2\Gamma_3}{\hbar} + k_{31}\right)k_{12}. \end{aligned} \tag{35}$$

Now, applying the inverse Laplace transformation to Eqs. (29)–(31), we obtain [19]

$$P_1(t) = A_1 e^{s_1 t} + A_2 e^{s_2 t} + A_3 e^{s_3 t}, \tag{36}$$

where

$$A_i = \frac{\left(s_i + \frac{2\Gamma_3}{\hbar} + k_{13}\right)\left(s_i + \frac{2\Gamma_2}{\hbar} + k_{12}\right)}{(s_i - s_k)(s_i - s_l))}, \tag{37}$$

$$P_2(t) = B_1 e^{s_1 t} + B_2 e^{s_2 t} + B_3 e^{s_3 t}, \tag{38}$$

where

$$B_i = k_{12}\frac{\left(s_i + \frac{2\Gamma_3}{\hbar} + k_{31}\right)}{(s_i - s_k)(s_i - s_l))}, \tag{39}$$

$$P_3(t) = C_1 e^{s_1 t} + C_2 e^{s_2 t} + C_3 e^{s_3 t}, \tag{40}$$

TABLE II. Computed quantum yields and $\tau_{ij} = 1/k_{ij}$ for *C. aurantiacus* RCs.

T	τ_{12}	τ_{21}	τ_{13}	τ_{31}	S^v_{12}	S^v_{13}	Φ_G	Φ_2	Φ_3
K	ps	ps	ps	ps					
300	1407	11111	8.8	30	18	5	0.05	0.01	0.94
80	25	2784	6.9	747	18	5	0.03	0.21	0.76
10	73	3268	8.1	895	18	5	0.04	0.10	0.86

where

$$C_i = k_{13}\frac{\left(s_i + \frac{2\Gamma_2}{\hbar} + k_{21}\right)}{(s_i - s_k)(s_i - s_l))}. \tag{41}$$

The occupation probabilities $P_i(t)$ are

$$P_1(t) = 0.0459e^{-0.4t} + 0.0003e^{-0.39t} + 0.9538e^{-0.16t}, \tag{42}$$

$$P_2(t) = -0.6081e^{-0.4t} + 0.0094e^{-0.39t} + 0.5988e^{-0.16t}, \tag{43}$$

$$P_3(t) = -0.0418e^{-0.4t} - 0.0184e^{-0.39t} + 0.0601e^{-0.16t}. \tag{44}$$

The numerical computations have been performing at 300 K for asymmetric case of the reorganization energies of the low frequency vibrational modes (first row in Table I), time t in ps, s_i in ps^{-1}; see Fig. 1.

V. ENERGIES SYMMETRY CASE

In this case, we assume that sites 2 and 3 have the same free energies. It means $\varepsilon_2 = \varepsilon_3$, and we assume only the asymmetry in reorganization energies of low-energy vibrational modes on branches L and M. We will investigate the influence of such asymmetry on the electron transfer directionality. To demonstrate this, the following values of input parameters were used in the numerical computations: the values of the scaled reorganization constants of low-frequency mode $S^v_{12} = 17$ and $S^v_{13} = 4$, the values of the scaled reorganization constants of high-frequency mode $S^h_{12} = S^h_{13} = 0.5$, high-frequency modes energy $\hbar\omega_h = 1500$ cm^{-1}, low-frequency mode energy $\hbar\omega_v = 55$ cm^{-1}. The values for electronic coupling parameters $V_{12} = V_{13} = 48$ cm^{-1} were used. The P^* internal conversion rate is $2\Gamma_1/\hbar = (170\ \text{ps})^{-1}$. The sink parameters $2\Gamma_2/\hbar = 2\Gamma_3/\hbar = 2.6$ ps and the site's free energies are $\varepsilon_{12} = \varepsilon_{13} = 460$ cm^{-1}. The calculated time τ_{ij} and quantum yields are collected in Table II. It can be seen that the asymmetry in the reorganization energies of the low-frequency modes cause unidirectionality in the high temperature regime ($T = 300$ K). At the low temperatures regime ($T = 80$ K, 10 K) this asymmetry causes asymmetry in the electron transfer but not the unidirectionality.

VI. NON-MARKOVIAN DESCRIPTION: NUMERICAL COMPUTATION

Here, we compare the kinetics of electron transfer described by the system of Eqs. (12)–(14) with the results obtained in the Markovian approximation Eqs. (36)–(41). To find the numeric solutions of the system of Eqs. (12)–(14) the IDESolver was used [20]. The package provides an interface for solving real- or complex-valued integrodifferential equations.

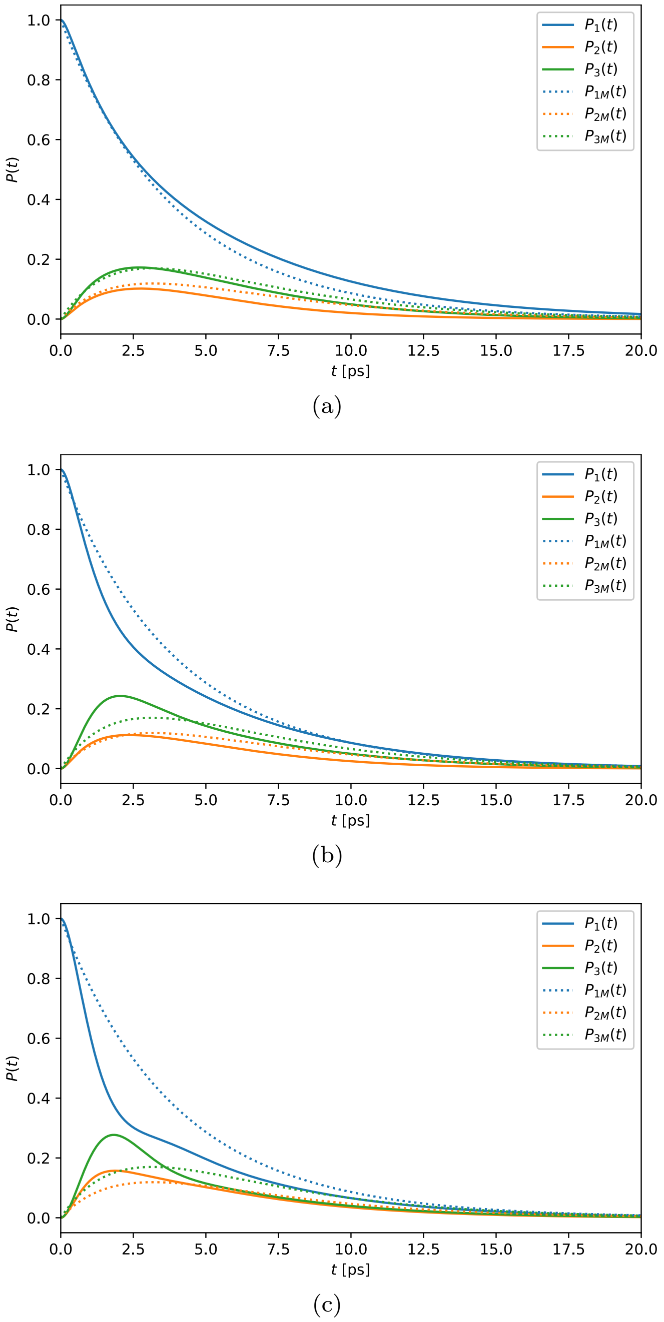

(a)

(b)

(c)

FIG. 2. The occupation probabilities $P_i(t)$ as a function of time t, solid lines represent the numerical calculation, dotted lines represents the Markovian approximation. Temperature $T = 300$ K, $\tau_p = 4.4$ ps (a), $\tau_p = 12.4$ ps (b), $\tau_p = 24.4$ ps (c).

Using the same phenomenological parameter τ_p for the numerical analysis as in Ref. [21], we have introduced the relaxation time for the vibrational mode $\omega_\alpha \to \omega_\alpha - i/\tau_p$, with the corresponding modification of Eq. (11) to

$$\mathcal{N}_\alpha(t) = (2\bar{n}_\alpha + 1)(1 - e^{-t/\tau_p}\cos\omega_\alpha t) + ie^{-t/\tau_p}\sin\omega_\alpha t. \tag{45}$$

In the computations, we used the following values of parameters: $S^h_{12} = S^h_{13} = 0.5$, $S^v_{12} = 17$, $S^v_{13} = 4$, $V_{12} = V_{13} =$

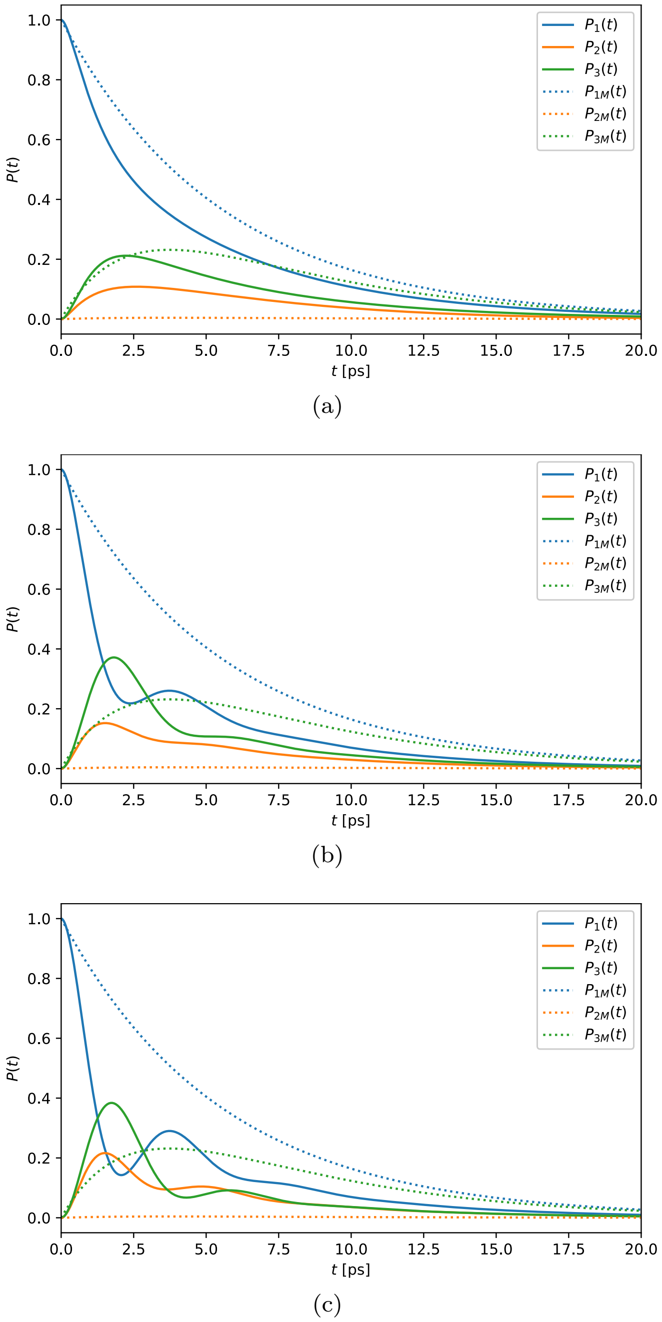

(a)

(b)

(c)

FIG. 3. The occupation probabilities $P_i(t)$ as a function of time t, solid lines represent the numerical calculation, dotted lines represents the Markovian approximation. Temperature $T = 10\,\mathrm{K}$, $\tau_p = 2.4\,\mathrm{ps}$ (a), $\tau_p = 12.4\,\mathrm{ps}$ (b), $\tau_p = 24.4\,\mathrm{ps}$ (c).

$48\,\mathrm{cm}^{-1}$, $V_{23} = 0$. The low-frequency mode energy $\hbar\omega_v = 80\,\mathrm{cm}^{-1}$ and the high-frequency mode energy in the range $\hbar\omega_h = 1500\,\mathrm{cm}^{-1}$ were used. Energy differences are $\varepsilon_{12} = \varepsilon_{13} = 460\,\mathrm{cm}^{-1}$. The sink parameters $\tau_i := (2\Gamma_i/\hbar)^{-1}$ were fixed for the values $\tau_1 = 170\,\mathrm{ps}$, $\tau_2 = \tau_3 = 2.6\,\mathrm{ps}$. The Markovian approximation gives:$\tau_{12} = 9.7$ ps, $\tau_{13} = 6.74$ ps at 300 K and $\tau_{12} = 306$ ps, $\tau_{13} = 5.8$ ps at 10 K.

On the plots of Figs. 2 and 3, one can see the comparison of numerical calculation and Markovian approximation for the occupation probabilities $P_i(t)$ as the function of time t for the temperatures $T = 300\,\mathrm{K}$ and $T = 10\,\mathrm{K}$ for different vibration relaxation times τ_p.

The numerical results show that at 300 K, the non-Markovian description and Markovian approximation give similar results for relaxation time $\tau_p = 4.4$ ps. For sufficiently long relaxation times (12.4ps, 24.4ps) the difference is apparent. The 10 K results give relatively similar results for time $\tau_p = 2.4$ ps. For long times, the difference is substantial. The electron transfer kinetics have a partially coherent character. The site occupation probability oscillates in time.

The Markovian approximation is correct when the dynamics of the system is slow in comparison to the rate of the loss of memory. It means that the minimum τ_{ij} ought to be bigger than τ_p. In our case, the minimum τ_{ij} is 6.74 ps at 300 K and 5.8 ps at 10 K. This can be the reason why the shorter vibration relaxation time is needed to get similar results in non-Markovian description and Markovian approximations at $T = 10$ K. For short vibration relaxation times, also in the non-Markovian description, the electron motion is incoherent. In this case, the memory function lost the memory faster than the electron moving from one site to another. In the case when the decay time of the memory function is longer than the minimum time τ_{ij} for the electron transfer between sites, the electron motion becomes coherent at the initial period.

VII. CONCLUSION

The coherent electron transport in RC may not be helpful. The increasing possibility of the backward electron transfer to the RC dimer exists in this case. And it increases the probability of the electron-hole recombination. The vibrational modes determine the electron transfer directionality. The interplay between electronic and vibration degrees of freedom is a crucial design parameter. The electron-vibronic coupling is used to localize the electrons on the needed site. To exhibit this statement, the electron transfer kinetics in the RCs of *C. aurantiacus* was investigated. It was shown that the asymmetry in the free energies and difference in reorganization energy of the low-frequency vibration mode of the L and M protein subunits can explain the unidirectionality of the electron transfer. The asymmetry in electronic coupling V_{ij} is not needed. The differences in the vibration reorganization energies can cause unidirectionality at high temperatures, but this assumption is not sufficient for unidirectionality at low temperatures. To explain the unidirectionality of the electron transfer in this RC, the Markovian approximation was used. The Markovian approximation can be used when the system dynamics are slower than the vibration relaxation time τ_p. The quantity τ_p lies beyond the scope of Markovian approximations. And so, the validity of the Markovian theory cannot be checked itself. So we have to count upon that relaxation process exist in the system of interest.

The data that support the findings of this articles are available within the article.

ACKNOWLEDGMENTS

The support of the Scientific Grant Agency of the Ministry of Education, Science, Research and Sport of the Slovak Republic and Slovak Academy of Sciences (VEGA) under Grant No. 2/0009/19 is acknowledged.

[1] *Quantum Effects in Biology*, edited by M. Mohseni, Y. Omar, G. S. Engel, and M. B. Plenio (Cambridge University Press, Cambridge, 2014).

[2] *Semiconductors and Semimetals*, edited by U. Würfel, M. Thorward, and E. R. Weber (Elsevier Inc., Amsterdam, 2011), Vol. 85.

[3] A. De Sio and Ch. Lienau, Phys. Chem. Chem. Phys. **19**, 18813 (2017).

[4] M. Pudlak and R. Pincak, Phys. Rev. E **68**, 061901 (2003).

[5] J. Cao, J. Chem. Phys. **112**, 6719 (2000).

[6] J. Wu and J. Cao, J. Chem. Phys. **139**, 044102 (2013).

[7] S. Nakajima, Prog. Theor. Phys. **20**, 948 (1958).

[8] R. Zwanzig, Physica **30**, 1109 (1964).

[9] M. Pudlak, J. Chem. Phys. **118**, 1876 (2003).

[10] A. J. Hoff and J. Deisenhofer, Phys. Rep. **287**, 1 (1997).

[11] J. A. Heller, D. Holten, and C. Kirmaier, Science **269**, 940 (1995).

[12] M. Pudlak and R. Pincak, Chem. Phys. Lett. **342**, 587 (2001).

[13] M. G. Müller, K. Griebenow, and A. R. Holzwarth, Biochimica et Biophysica Acta (BBA) - Bioenergetics **1098**, 1 (1991).

[14] M. Pudlak and R. Pincak, J. Biol. Phys. **36**, 273 (2010).

[15] M. A. Harris *et al.*, J. Phys. Chem. B **117**, 4028 (2013).

[16] M. Pudlak and R. Pincak, Eur. Phys. J. E **34**, 22 (2011).

[17] Z. Guo, S. Lin, Y. Xin, H. Wang, R. E. Blankenship, and N. W. Woodbury, J. Phys. Chem. B **115**, 11230 (2011).

[18] M. Becker, V. Nagarajan, D. Middendorf, W. W. Parson, J. E. Martin, and R. E. Blankenship, Biochim. Biophys. Acta **1057**, 299 (1991).

[19] G. A. Korn and T. M. Korn, *Mathematical Handbook* (McGraw-Hill, New York, 1968).

[20] J. T. Karpel, JOSS **3**, 542 (2018).

[21] M. Pudlak, K. N. Pichugin, R. G. Nazmitdinov, and R. Pincak, Phys. Rev. E **84**, 051912 (2011).